JBC RESEARCH ARTICLE

Identification of invariant chain CD74 as a functional receptor of tissue inhibitor of metalloproteinases-1 (TIMP-1)

Received for publication, June 28, 2021, and in revised form, August 4, 2021 Published, Papers in Press, August 12, 2021,
https://doi.org/10.1016/j.jbc.2021.101072

Benjamin Schoeps[1,‡], Celina Eckfeld[1,‡], Laura Flüter[1], Selina Keppler[2,3], Ritu Mishra[2,3], Percy Knolle[1], Felix Bayerl[1], Jan Böttcher[1], Chris D. Hermann[1], Daniel Häußler[1], and Achim Krüger[1,*]

From the [1]School of Medicine, Institutes of Molecular Immunology and Experimental Oncology, [2]School of Medicine, Institute of Clinical Chemistry and Pathobiochemistry, [3]TranslaTUM, Center for Translational Cancer Research, Technical University Munich, Munich, Germany

Edited by Henrik Dohlman

Multifunctionality of tissue inhibitor of metalloproteinases-1 (TIMP-1) comprising antiproteolytic as well as cytokinic activity has been attributed to its N-terminal and C-terminal domains, respectively. The molecular basis of the emerging proinflammatory cytokinic activity of TIMP-1 is still not completely understood. The cytokine receptor invariant chain (CD74) is involved in many inflammation-associated diseases and is highly expressed by immune cells. CD74 triggers zeta chain–associated protein kinase-70 (ZAP-70) signaling–associated activation upon interaction with its only known ligand, the macrophage migration inhibitory factor. Here, we demonstrate TIMP-1–CD74 interaction by coimmunoprecipitation and confocal microscopy in cells engineered to overexpress CD74. *In silico* docking in HADDOCK predicted regions of the N-terminal domain of TIMP-1 (N-TIMP-1) to interact with CD74. This was experimentally confirmed by confocal microscopy demonstrating that recombinant N-TIMP-1 lacking the entire C-terminal domain was sufficient to bind CD74. Interaction of TIMP-1 with endogenously expressed CD74 was demonstrated in the Namalwa B lymphoma cell line by dot blot binding assays as well as confocal microscopy. Functionally, we demonstrated that TIMP-1–CD74 interaction triggered intracellular ZAP-70 activation. N-TIMP-1 was sufficient to induce ZAP-70 activation and interference with the cytokine-binding site of CD74 using a synthetic peptide–abrogated TIMP-1-mediated ZAP-70 activation. Altogether, we here identified CD74 as a receptor and mediator of cytokinic TIMP-1 activity and revealed TIMP-1 as moonlighting protein harboring both cytokinic and antiproteolytic activity within its N-terminal domain. Recognition of this functional TIMP-1–CD74 interaction may shed new light on clinical attempts to therapeutically target ligand-induced CD74 activity in cancer and other inflammatory diseases.

Tissue inhibitor of metalloproteinases-1 (TIMP-1) is a soluble metalloproteinase inhibitor, which is found at high concentrations in the circulation of patients suffering from inflammation-associated diseases (1–3). Originally described as the first natural collagenase inhibitor (4), it was revealed that TIMP-1 is identical to erythroid-potentiating activity (5), a potent growth factor for erythroid progenitors. Subsequent studies revealed further effects of TIMP-1 on cells of the hematopoietic system, including B lymphoma cells (6–8). Interestingly, many of the observed TIMP-1-mediated effects were shown to be independent of its antiproteolytic activity (6, 9), which so far was the only major function exhibited by the N-terminal domain (10). Several years later, it was discovered that C-terminal domain–mediated interaction of TIMP-1 with the tetraspanin CD63 (11, 12) induces proteolysis-independent cytokinic signaling resulting in a variety of protumorigenic, prometastatic, and proinflammatory effects (13–16). Hence, the multifunctionality of TIMP-1 was attributed to the existence of two physically distinct domains, the N-terminal domain mediating antiproteolytic activity as well as the C-terminal domain mediating signaling activity *via* CD63 (17).

In an abstract for a symposium, without provision of experimental data (18), it was suggested that invariant chain (CD74) may be a possible interaction partner of TIMP-1. CD74 is, like TIMP-1, associated with inflammatory diseases (19) and is discussed as a therapeutic target in cancer (20) and autoimmune diseases (21) and notably also in the ongoing SARS-CoV-2 pandemic (22). CD74 plays an essential role in many biological processes (23), including antigen presentation (24) and B cell development (25). Homotrimers of CD74 bind major histocompatibility complex (MHC) class II complexes to assist their assembly and subcellular localization (23, 26). In addition, MHC-free CD74 can also be found on the surface of immune cells (23, 27), where it serves as the receptor for the cytokine macrophage migration inhibitory factor (MIF) (28). Functionally, the MIF–CD74 interaction was shown to induce intracellular zeta chain–associated protein kinase-70 (ZAP-70) signaling in B lymphoma cells (29). In the present study, we identified CD74 as a functionally active receptor for TIMP-1, mediating cytokinic signaling activity of TIMP-1. Furthermore, we identified the antiproteolytic N-terminal domain of TIMP-1 to be a functional cytokinic interaction site as well.

‡ These authors contributed equally to this work.
* For correspondence: Achim Krüger, achim.krueger@tum.de.

Results

TIMP-1 interacts with CD74

To investigate a possible TIMP-1–CD74-interaction, we overexpressed CD74 in the human LX-2 cell line, which resulted in highly increased RNA (Fig. 1*A*), total protein (Fig. 1*B*), as well as surface protein (Fig. 1*C*) levels of CD74. Physical interaction between TIMP-1 and CD74 could be demonstrated by coimmunoprecipitation using the crude lysate of CD74-overexpressing cells (Fig. 1*D*). Furthermore, colocalization of fluorescently labeled TIMP-1 with CD74 was observed (Fig. 1*E*). Altogether, these data show that TIMP-1 binds to CD74.

In silico *prediction of TIMP-1–CD74 interacting residues by molecular docking*

To shed light on possible interaction sites involved in TIMP-1–CD74 binding, we performed *in silico* molecular docking using the Haddock algorithm (30), which predicts the most likely conformation of two interacting molecules (Fig. 2*A*). For this, we used the full-length crystal structure of TIMP-1 (PDB ID: 1uea) (31) and the trimerized extracellular domain of CD74 (PDB ID: 1iie) (32). Of 10,000 randomly assigned interactions between TIMP-1 and CD74, the 200 energetically most favorable interactions were further refined by semiflexible annealing. The structures of these refined TIMP-1–CD74 complexes were compared and complexes with similar orientation were clustered. Of the resulting 22 clusters, the three, in respect to energetic considerations, best-ranked clusters (clusters 2, 8, and 13 (Table S1)) were further analyzed.

To gain more insight in the binding sites that are involved in TIMP-1–CD74 interaction, we visualized a representative complex structure for each cluster (complex 2, complex 8, and complex 13) (Fig. 2*B*) and used the SpotOn algorithm, which identifies and classifies interfacial residues of protein–protein interactions (33, 34). This analysis revealed that, in complexes 8 and 13, TIMP-1 would interact with CD74 mainly *via* its N-terminal domain (Fig. 2*B*), including the wedge-shaped ridge at the N terminus of TIMP-1 (Fig. 2*C* and Fig. S1*A*). This interaction was predicted to involve all three monomers of the CD74 homotrimer (Fig. 2*D* and Fig. S1*B*). In contrast, complex 2 suggested binding to CD74 only *via* the C-terminal domain of TIMP-1 (Fig. 2, *B* and *C* and Fig. S1*A*).

Interestingly, some of the suggested residues on CD74 that participate in the interaction with TIMP-1 (highlighted in Fig. S1*B*) were previously also predicted to be involved in binding of the MIF to CD74 (35).

In vitro *validation of the* in silico*–predicted docking site of TIMP-1 with CD74*

The *in silico* analysis suggested two possible binding orientations of TIMP-1 to CD74. First, binding to CD74 would be mediated *via* the N-terminal domain of TIMP-1 (complex 8 and complex 13). Second, the interaction with CD74 would be mediated *via* the C-terminal domain of TIMP-1 (complex 2). To experimentally validate one of the proposed binding mechanisms, we deleted the C-terminal domain of TIMP-1 and used the purified N-terminal domain (N-TIMP-1) for *in vitro* studies. Confocal microscopy revealed that N-TIMP-1, similar to full-length TIMP-1 (Fig. 1*B*), colocalized with CD74 (Fig. 3*A*). This experimental approach demonstrates that the N-terminal domain of TIMP-1 is sufficient to bind to CD74, supporting the binding mechanism suggested by complexes 8 and 13.

As a proof of concept, we aimed to investigate whether the identified TIMP-1–CD74 interaction also occurs in cells with natural expression of CD74. Analysis of published RNA-Seq data derived from the human protein atlas (36) revealed that cells in the immune cell compartment, particularly B cells, highly expressed *CD74* (Fig. S2). Therefore, we used the Namalwa human B lymphoma cell line, which highly expressed CD74 (Fig. S3*A*), for further studies on TIMP-1–CD74 interactions. Dot blot binding assays using cell lysates of Namalwa cells revealed, in comparison with the negative control BSA, markedly increased binding of CD74 to immobilized recombinant TIMP-1 to a similar extent as the positive control recombinant MIF (Fig. 3*B*). This increase was totally abolished when TIMP-1-coated dots were incubated with lysates from CD74 knockdown cells (Fig. 3*B* and Fig. S3, *B* and *C*). Furthermore, colocalization of fluorescently labeled TIMP-1 and CD74 in intact Namalwa cells was observed using confocal microscopy (Fig. 3*C*). Importantly, N-TIMP-1 was sufficient to bind to Namalwa-derived CD74 (Fig. 3*D*).

TIMP-1–CD74 interaction induces ZAP-70 signaling

Next, we examined whether the identified TIMP-1–CD74 interaction is functional. For this, we analyzed phosphorylation of ZAP-70, a known downstream effector of CD74 signaling in B lymphoma cells upon binding of MIF (29). Stimulation of Namalwa cells with recombinant TIMP-1 triggered ZAP-70 phosphorylation (Fig. 4*A*). Importantly, TIMP-1-mediated ZAP-70 phosphorylation was dependent on CD74 because shRNAi-mediated knockdown of CD74 (Fig. 4*B*) completely abolished this effect (Fig. 4*C*). Of note, GAPDH and total ZAP-70 levels were not affected by TIMP-1 stimulation (Fig. S4). To further analyze the relevance of the above-identified interfacial residues of TIMP-1–CD74 interaction, we stimulated Namalwa cells with N-TIMP-1 and observed that the N-terminal domain was sufficient to trigger ZAP-70 phosphorylation (Fig. 4*D*). The abovementioned complexes 8 and 13, which were identified to reflect the most probable binding mechanism, predicted a TIMP-1-binding region on CD74 that is similar to the previously published binding region of MIF on CD74 (35). Because MIF–CD74 interaction can be blocked with the synthetic CD74-binding peptide C36L1 occupying this binding region on CD74 (37), we used C36L1 to test for the plausibility of the *in silico*–revealed TIMP-1-interaction regions on CD74. Indeed, preincubation of cells with this peptide abolished TIMP-1–CD74-mediated ZAP-70 phosphorylation (Fig. 4*E*), indicating that the known cytokine-binding site on CD74 is involved in TIMP-1–CD74

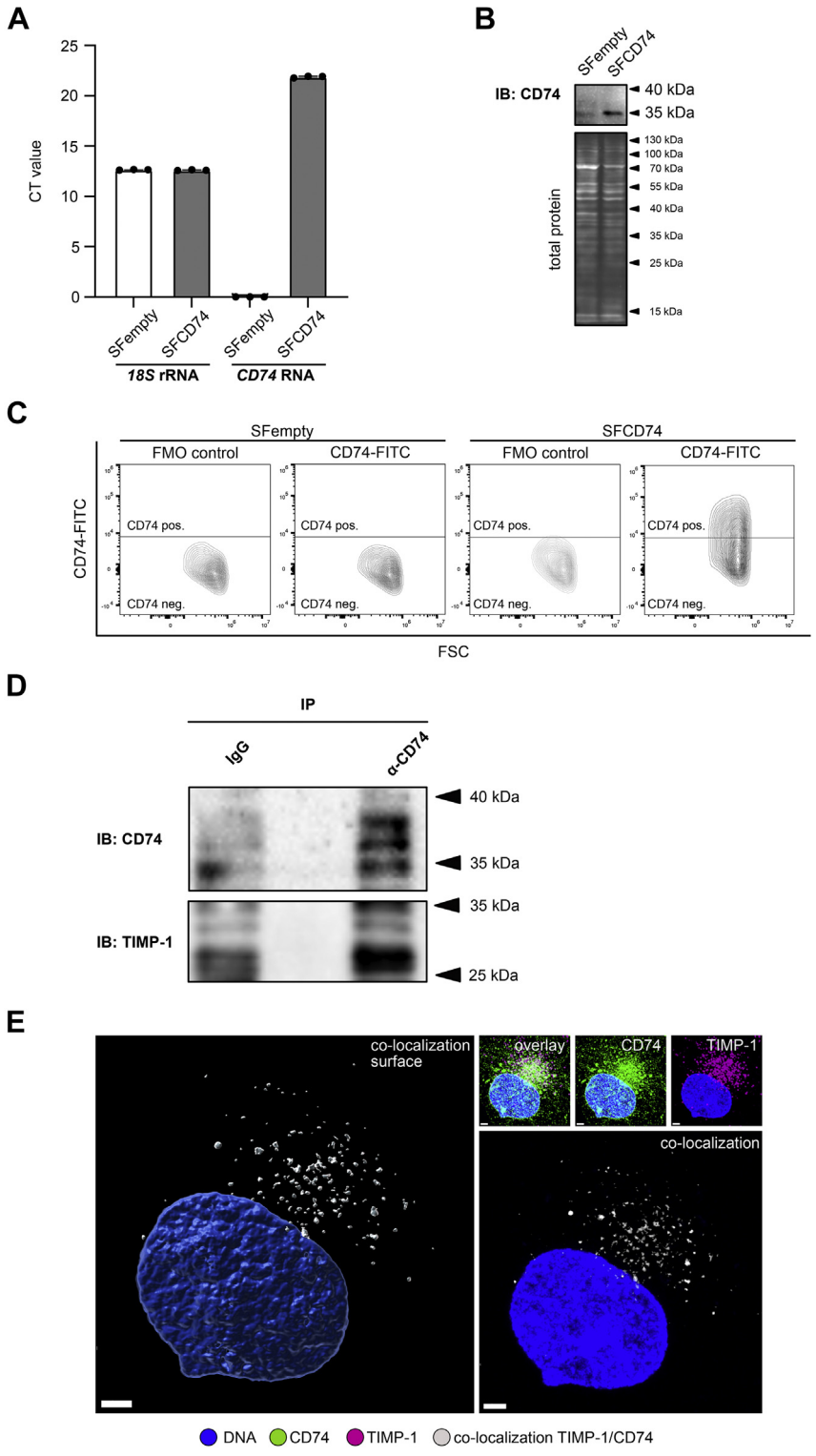

Figure 1. TIMP-1 interacts with CD74. *A*, qRT-PCR analysis of *18S* rRNA and *CD74* RNA expression in control (SFempty) and CD74-overexpressing (SFCD74) LX-2 cells. Results are represented as the mean ± SD of three technical replicates. *B*, representative Western blot detecting human CD74 in control (SFempty) and CD74-overexpressing (SFCD74) LX-2 cells. Equal protein loading was examined by whole-protein staining by SYPRO Ruby protein stain. *C*, representative contour plots showing cell populations of SFempty and SFCD74 LX-2 cells after exclusion of cell debris and dead cells. Fluorescence-minus-one (FMO) controls and CD74-FITC stained cells are shown, respectively. CD74-FITC fluorescence intensity (y-axis) is plotted against forward scatter (FSC) values. Indicated CD74-positive gates were set in FMO controls of each cell line. *D*, representative coimmunoprecipitation of CD74 and TIMP-1. Agarose beads conjugated with anti-CD74 antibodies or control IgG-conjugated beads were incubated with the nondenatured cell lysate derived from CD74 overexpressing cells, and protein abundance in pull-down fractions was analyzed *via* Western blot. *E*, representative confocal image of CD74-overexpressing LX-2 cells stimulated with fluorescently labeled recombinant human TIMP-1 (Alexa^{555}-TIMP-1). The nucleus is shown in *blue*, Alexa^{555}-TIMP-1 is shown in *magenta*, and CD74 is shown in *green*. Regions of TIMP-1–CD74 colocalization are shown in *gray*. The scale bars represent 3 μm. TIMP-1, tissue inhibitor of metalloproteinases-1.

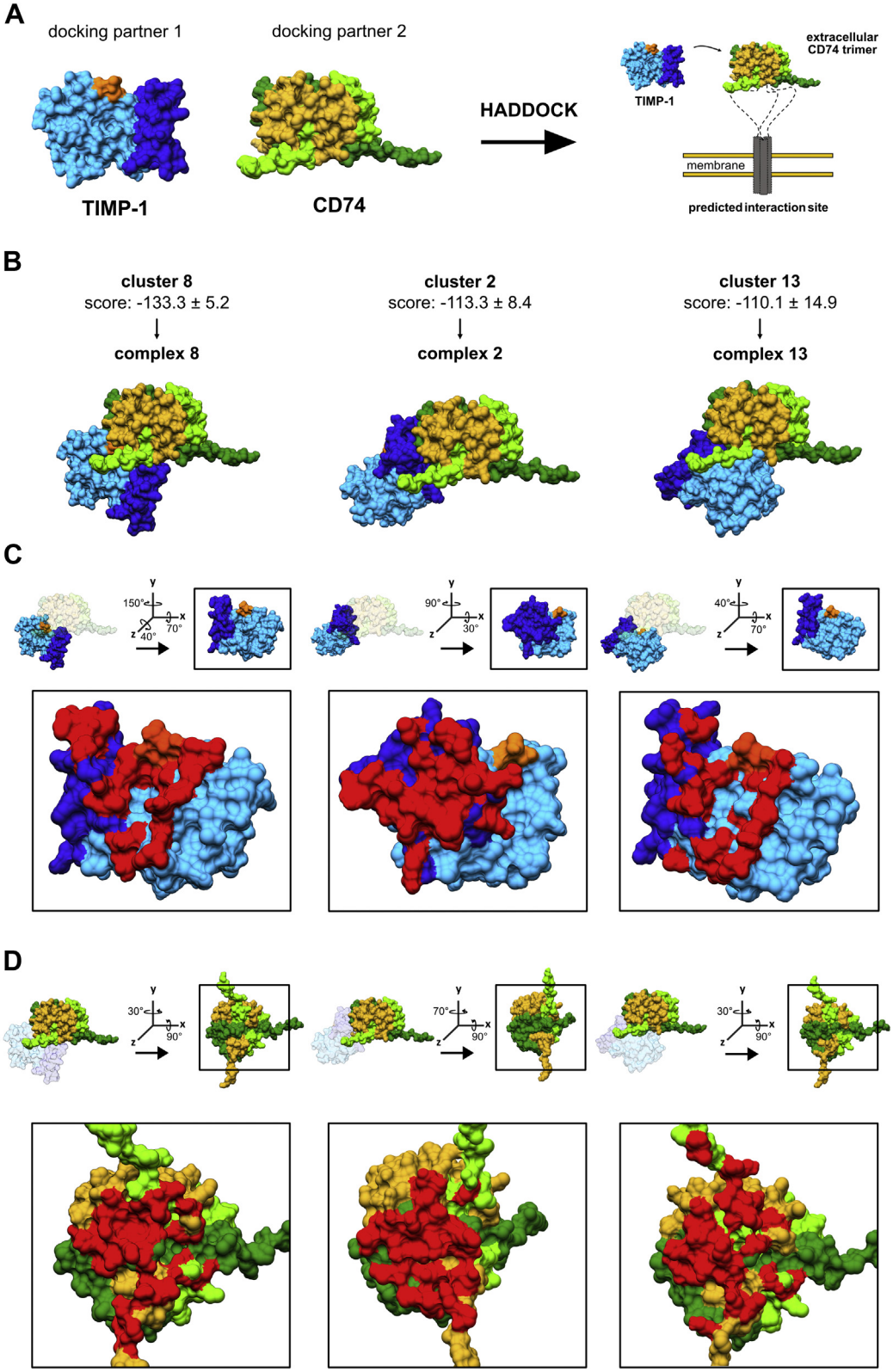

Figure 2. *In silico* prediction of TIMP-1–CD74 interacting residues by molecular docking. *A*, illustration of the molecular docking approach to predict the interaction site of TIMP-1 (PDB ID: 1uea) with CD74 (PDB ID: 1ile). Known crystal structures are shown in surface depiction, and *dashed lines* indicate unresolved structural regions. *B*, representative complexes of the three energetically most favorable TIMP-1–CD74 clusters obtained from the haddock docking approach and illustrated with UCSF Chimera. The N-terminal domain of TIMP-1 is shown in *light blue*, the C-terminal domain is shown in *blue*, and the CTC motif of TIMP-1 is shown in *orange*. Monomer 1 of the CD74 homotrimer is shown in *dark green*, monomer 2 is shown in *light green*, and monomer 3 is shown in *yellow*. The indicated score represents the respective calculated Haddock score, an indicator of the intermolecular energy of the respective complexes. *C*, surface representation of TIMP-1 with interface regions participating in the interaction with CD74 highlighted in *red*. The CTC motif is highlighted in *orange* (*top*). TIMP-1 molecules were turned around the x, y, and z axes as indicated. *D*, surface representation of CD74 with interface regions participating in the interaction with TIMP-1 highlighted in *red*. CD74 molecules were turned around the x, y, and z axes as depicted.

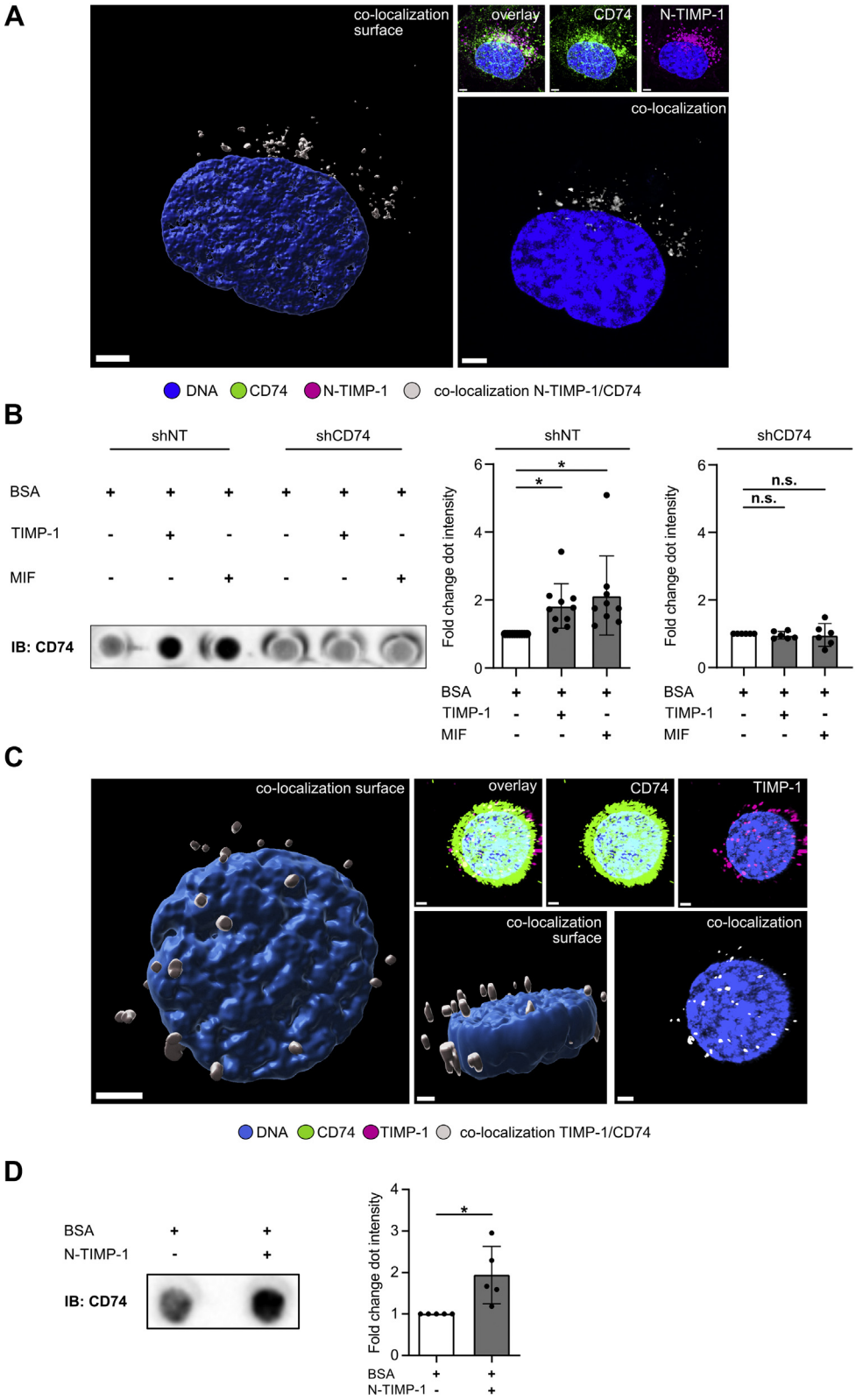

Figure 3. *In vitro* validation of the *in silico*–predicted docking site of TIMP-1 with CD74. *A*, representative confocal image of CD74-overexpressing LX-2 cells stimulated with fluorescently labeled recombinant human N-TIMP-1 (Alexa^{555}N-TIMP-1). The nucleus is shown in *blue*, Alexa^{555}N-TIMP-1 is shown in *magenta*, CD74 is shown in *green*. Regions of N-TIMP-1–CD74 colocalization are shown in *gray*. The scale bars represent 4 μm. *B*, representative dot blot assay showing the binding of endogenous CD74 derived from nondenatured B lymphoma cell lysates (shNT or shCD74) to immobilized TIMP-1 or MIF, respectively. Binding of cell lysate–derived CD74 to uncoated (shNT: n = 10, shCD74: n = 5), TIMP-1-coated (shNT: n = 10, shCD74: n = 5), and MIF-coated (shNT: n = 9, shCD74: n = 5) dots was determined by immunoblotting against CD74 (*left*) and quantified using densitometric analysis of dots (*right*). *C*, representative confocal image of a B lymphoma cell stimulated with fluorescently labeled recombinant human TIMP-1 (Alexa^{555}TIMP-1). Distribution of TIMP-1 (*magenta*), CD74 (*green*), as well as TIMP-1–CD74 colocalization (*white*) is shown. Surfaces of TIMP-1–CD74 colocalization are displayed in *gray*, and

interaction. Of note, we could exclude effects of the peptide on cell viability during the time frame of the experiment (Fig. S5).

Discussion

In this study, we identified CD74 as the functional receptor of TIMP-1. Interaction of TIMP-1 with CD74 was observed in lysates derived from cells of different origins, namely CD74-overexpressing hepatic stellate cells as well as Namalwa B lymphoma cells with natural expression of CD74. This finding was further supported by confocal microscopy revealing that fluorescently labeled exogenous TIMP-1 binds to the receptor CD74. The observation that not all TIMP-1 molecules colocalized with CD74 in cells points at additional TIMP-1-binding proteins. Indeed, several cell surface proteins are known to bind TIMP-1, including CD63 (11), LRP-1 (38, 39), and ADAM10 (40).

Further molecular analyses on the identified interaction between TIMP-1 and CD74 led to the observation that TIMP-1 interacts with CD74 *via* its N-terminal domain because N-TIMP-1 alone was sufficient to bind to CD74 as well as trigger ZAP-70 activation. Still, molecular docking analyses indicated that some amino acids located in the C-terminal domain facing the wedge-shaped ridge of TIMP-1 (41) possibly participate in the interaction with CD74 as well. Therefore, it is possible that these residues can be involved in modulation of the TIMP-1–CD74 interaction. Such contribution of amino acids of the C-terminal domain to the binding of TIMP-1 to other known N-terminal interaction partners has already been described in the context of its antiproteolytic activity because residues in the C-terminal domain are not decisive for, but involved in, fine-tuning of TIMP-1–metalloproteinase interactions (42, 43).

TIMP-1 is a multifunctional protein with versatile impact on cellular processes. Its functions result from its two-domain structure harboring metalloproteinase inhibitory as well as cytokine activities (17). So far, the N-terminal domain of TIMP-1 was almost entirely recognized to be responsible for the antiproteolytic function (10), while it emerged that the C-terminal domain is the mediator of its cytokinic activity (11, 12). This appreciation now has to be revised as we here demonstrate that the N-terminal domain of TIMP-1 binds to CD74 and triggers ZAP-70 activation in Namalwa B lymphoma cells. Thus, the multifunctionality of TIMP-1 expands beyond functional separation of two distinct domains because the N-terminal domain harbors both metalloproteinase inhibitory and cytokinic functions.

CD74 is, like TIMP-1, highly expressed in inflammatory conditions (19) and has been shown to be involved in a multitude of biological processes (23), including antigen presentation (24) and cellular signaling (29). So far, the only known ligand of CD74 was the proinflammatory cytokine MIF, and MIF–CD74 interaction was shown to induce ZAP-70 signaling in B lymphoma cells (29). The clinical relevance of ligand-induced CD74 activity is demonstrated by clinical trials using anti-CD74 antibodies for the therapy of malignant B cell lymphoma (44) as well as studies aiming at interference with CD74–MIF signaling in the ongoing SARS-CoV-2 pandemic (22). Our finding that ZAP-70 signaling is also triggered upon interaction of TIMP-1 with CD74 suggests that TIMP-1 and MIF may exert similar cellular responses. Interestingly, the molecular modeling analyses suggested that TIMP-1 binds to the known MIF-binding site on CD74 (35, 37). This was experimentally validated by interference with TIMP-1–CD74 signaling using a peptide known to block MIF–CD74 interaction (37). The physiological consequence of TIMP-1–CD74 interactions, including a potential competition between TIMP-1 and MIF in binding to CD74, warrants further investigation.

In conclusion, our findings render TIMP-1 as a moonlighting protein (45), where the N-terminal domain harbors both the well-known antiproteolytic activity and a so far unknown signaling function.

Experimental procedures

Cell lines

The human LX-2 cell line was cultured in DMEM (Biochrom AG) supplemented with 2% fetal bovine serum, 1% glutamine, and 2% penicillin/streptomycin at 37 °C and 5% CO_2. The human B lymphoma cell line Namalwa was cultured in RPMI 1640 (Thermo Fisher Scientific Inc) supplemented with 7.5% fetal bovine serum.

Generation of stable cell lines using lentiviral gene transfer

Knockdown of CD74

Experimental procedures were followed as described previously (46). Briefly, 5×10^6 293T cells were seeded in 10-cm dishes. After 1 day, media were replaced and cotransfection of transfer plasmids purchased from Sigma Aldrich (shCD74 #1 (TRCN0000008636, 96.65% knockdown, validated), shCD74 #2 (TRCN0000008635, 98.35% knockdown, validated), shCD74 #3 (TRCN0000008639, 74.14% knockdown, validated), (for knockdown efficiencies, see Fig. 4*B* and Fig. S3, *B* and *C*)) with lentiviral packaging plasmids (pMD.GP, pRSV-rev, pMD.G) was performed using Lipofectamine 2000 (cat.#11668019, Thermo Fisher Scientific Inc). shRNA that does not target any known human or mouse gene (shNT) was used as a control. Two days later, lentiviral particles were harvested from the supernatant and frozen at −80 °C. Target cells were infected with lentiviral particles in presence of 8 μg/ml Polybrene (cat.#TR-1003-G, Sigma Aldrich), and selection of transduced cells was performed using 10 μg/ml puromycin.

the nucleus is shown in *blue*. The scale bars represent 2 μm. *D*, representative dot blot assay investigating N-TIMP-1 binding to CD74. Immobilized N-TIMP-1 was incubated with nondenatured cell lysate from B lymphoma cells. Binding of cell lysate-derived CD74 to uncoated (n = 5) and N-TIMP-1-coated dots (n = 5) was determined by immunoblotting against CD74 (*left panel*) and quantified using densitometric analysis of dots (*right panel*). *B* and *D*, results are represented as the mean ± SD. For statistical analyses, a one-sample *t* test was used in case of normal distribution or a one-sample Wilcoxon test in absence of normal distribution, $*p \leq 0.05$. MIF, macrophage migration inhibitory factor; N-TIMP-1, N-terminal domain of TIMP-1; TIMP-1, tissue inhibitor of metalloproteinases-1.

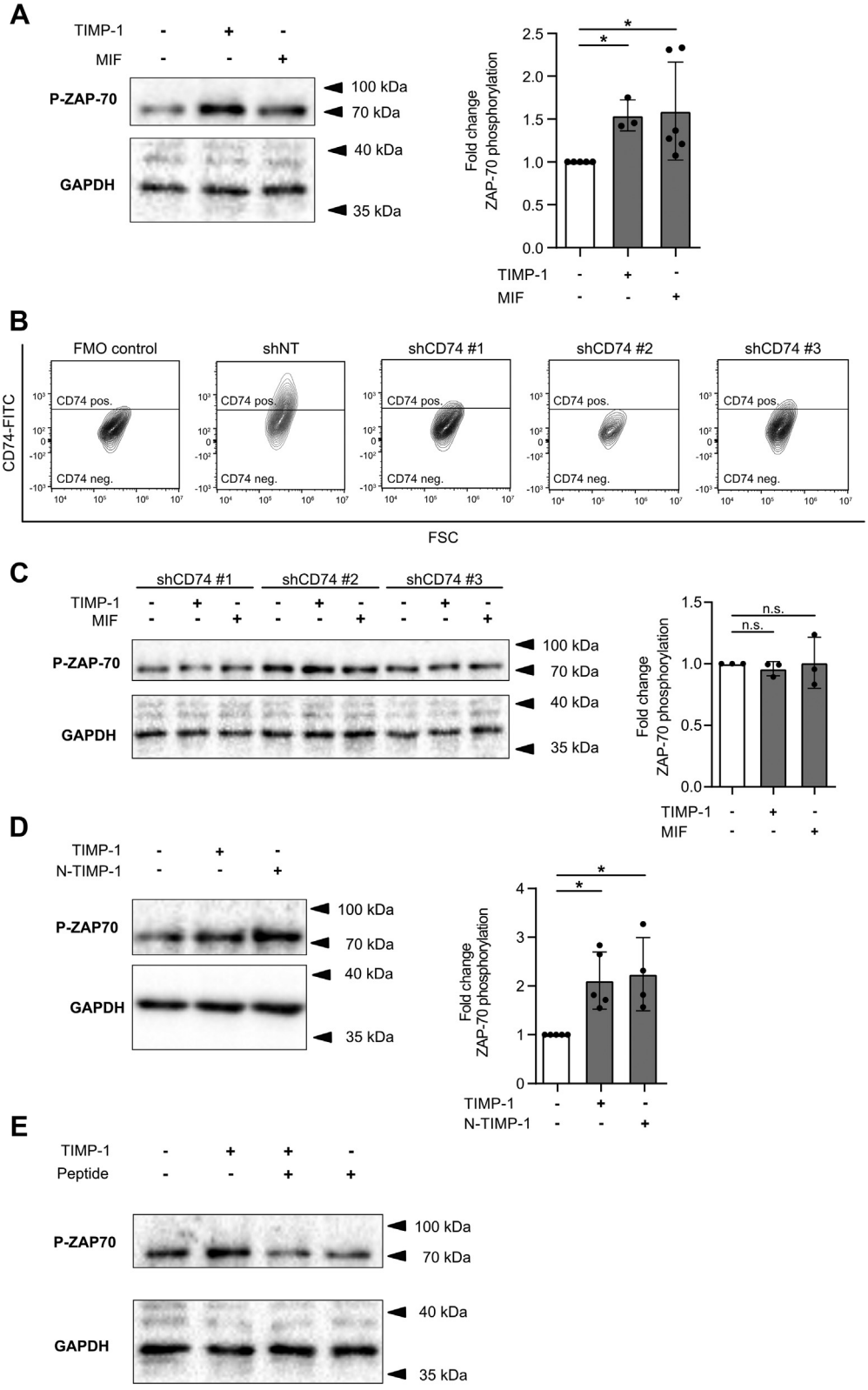

Figure 4. TIMP-1–CD74 interaction induces ZAP-70 signaling. *A*, *C*, *D*, and *E*, representative Western blots of cell lysates from B lymphoma cells treated as indicated. Levels of phosphorylated ZAP-70 and GAPDH were analyzed. *A*, cells were treated with 500 ng/ml human recombinant WT TIMP-1 (n = 3), 100 ng/ml human recombinant MIF (n = 6) or were left untreated (n = 4) (*left*). Fold change of ZAP-70 activation was determined by densitometric analysis of band intensities normalized to levels of GAPDH (*right*). *B*, representative flow cytometric analysis of CD74 expression by three different CD74 knockdown B lymphoma cells (shCD74 #1, #2, #3) or control cells (shNT). Contour plots show the frequency of CD74-positive cells. *C*, representative Western blots of cell lysates from three different CD74 knockdown B lymphoma cells (shCD74 #1, #2, #3) or control cells (shNT) treated as indicated. *D*, B lymphoma cells were stimulated with 500 ng/ml human recombinant TIMP-1 (n = 5), equimolar human recombinant N-TIMP-1 (n = 4), or left untreated (n = 5) (*left*). Fold change of ZAP-70 activation was determined by densitometric analysis of band intensities normalized to levels of GAPDH (*right*). *E*, B lymphoma cells were

Overexpression of CD74

CD74-overexpressing LX-2 cells were generated using a lentiviral vector (plasmid pHIV7) containing a spleen focus-forming promoter for overexpression of the *CD74* isoform p33. The DNA sequence of *CD74* was synthesized by Invitrogen GeneArt Gene Synthesis (Thermo Fisher Scientific Inc). Control cells were generated using an empty vector.

Stimulation of cells and interference

Recombinant human (N-)TIMP-1 was expressed in an endotoxin-free mammalian cell culture system of HEK293F cells (Thermo Fisher Scientific) and purified in a three-step protocol using an Äktapure Fast Protein Liquid Chromatography system (Cytiva) as described previously (16). For stimulation of cells for subsequent analysis of intracellular signaling, cells were incubated in serum-free media containing 0.1% BSA for 24 h before stimulation. After serum starvation, cells were exposed to pathophysiological concentrations of TIMP-1 (500 ng/ml) (14), N-TIMP-1 (392 ng/ml, equimolar to TIMP-1), or MIF (100 ng/ml, Abcam, cat. #ab75432) for 10 min and whole-cell extracts were isolated using RIPA lysis buffer (50 mM Tris/HCl, pH 7.4, 150 mM NaCl, 0.25% SDS, 1% NP-40, 1 mM EDTA) supplemented with protease and phosphatase inhibitors (Carl Roth). Concentrations of isolated proteins were determined using the Pierce BCA Protein Assay Reagents (Thermo Fisher Scientific Inc). For interference with TIMP-1–CD74–mediated signaling, cells were preincubated with the CD74-blocking peptide C36L1 (37) (200 μM, KSSQSVFYSSNNKNYLA-NH2, peptides & elephants GmbH) for 6 h before stimulation.

Coimmunoprecipitation

For coimmunoprecipitation experiments, nondenatured cell lysates of TIMP-1-stimulated (500 ng/ml) CD74-overexpressing LX-2 cells were prepared by a nondenaturing cell lysis buffer (20 mM Tris HCl, pH 8, 137 mM NaCl, 1% NP-40, 2 mM EDTA, including phosphatase and proteinase inhibitors). Cell lysates were incubated with agarose beads conjugated with anti-CD74 (cat.# sc-6262-AC, Santa Cruz Biotechnology) or IgG antibodies (cat.# sc-2343-AC, Santa Cruz Biotechnology). Before incubation with cell lysates, conjugated beads were blocked for 1 h at room temperature (RT) with 5% BSA in PBS to avoid unspecific binding. Beads were then centrifuged (1000*g*, 30 s, 4 °C) and washed three times with PBS. The remaining cell pellet was resuspended in the nondenatured cell lysate of CD74-overexpressing LX-2 cells and incubated overnight at 4 °C while rotating. After centrifugation (1000*g*, 30 s, 4 °C) and washing (3× with PBS), the remaining cell pellet containing the beads and bead-bound molecules were resuspended in the loading buffer (0.2 M Tris, 0.03% SDS, 0.07% glycerin, 0.002% bromophenol blue, 0.05% β-mercaptoethanol) and boiled at 95 °C for 5 min to elute bound molecules from the beads. Eluates were then subjected to Western blot analysis to detect protein abundance of CD74 and TIMP-1.

Western blot

For Western blot analyses, equal amounts of protein were resuspended in the loading buffer (0.2 M Tris, 0.03% SDS, 0.07% glycerin, 0.002% bromophenol blue, 0.05% β-mercaptoethanol) and incubated for 5 min at 95 °C. Samples were centrifuged (13,000*g*, 3 min, 4 °C) and separated by a 10% or 12.5% SDS PAGE. Proteins were transferred onto a nitrocellulose membrane (Amersham Bioscience) using a Trans-Blot semidry blotting system (Bio-Rad Laboratories Inc). After protein transfer, membranes were blocked with 5% BSA in TBS-T (1× TBS containing 0.1% Tween 20) for 1 h at RT and incubated with primary antibodies against P-ZAP-70 (Tyr319, cat. #2701S, Cell Signaling Technology), human CD74 (1:1000, # sc-20082, Santa Cruz Biotechnology), or GAPDH (cat. #sc-25778, Santa Cruz Biotechnology) diluted in 5% BSA in TBS-T overnight at 4 °C. Membranes were washed three times with TBS-T at RT and incubated with secondary goat anti-rabbit IgG HRP-conjugated antibody solutions (1:5000; cat. #31462, Thermo Fisher Scientific Inc) for 1 h at RT. Membranes were washed three times with TBS-T, and bands were visualized using the Pierce ECL substrate (Thermo Fisher Scientific Inc). Bands were detected and quantified using the ChemiDoc imaging system (Bio-Rad Laboratories Inc) and the ImageLab Software (Bio-Rad Laboratories Inc).

Chemiluminescent dot blot binding assay

Binding of CD74 to TIMP-1, N-TIMP-1, and MIF was analyzed by chemiluminescent Dot blot assays. Human recombinant TIMP-1 (6.7 μg), N-TIMP-1 (equimolar concentrated), and MIF (equimolar concentrated), diluted in TBS buffer, were immobilized on a nitrocellulose membrane using a Bio-Dot microfiltration apparatus (Bio-Rad Laboratories Inc) according to the manufacturer's instructions. Uncoated dots were incubated with TBS buffer only. All dots were blocked with 5% BSA in TBS-T and incubated overnight at 4 °C with nondenatured cell lysates derived from the B lymphoma cell line Namalwa (20 μg/ml). Cell lysis was performed using a nondenaturing cell lysis buffer (20 mM Tris HCl, pH 8.0, 137 mM NaCl, 1% Triton X-100, 2 mM EDTA). Membranes were washed twice with TBS-T, incubated with primary antibodies against human CD74 (1:1000, # sc-20082, Santa Cruz Biotechnology) until the antibody solution was drained through the wells completely. Membranes were washed twice with TBS-T and incubated with secondary goat anti-rabbit IgG HRP-conjugated antibody solutions (1:5000; cat. #31462, Thermo Fisher Scientific Inc). After washing with TBS-T, dots were visualized using the ChemiDoc imaging system (Bio-Rad

stimulated with 500 ng/ml TIMP-1 after preincubation with or without an anti-CD74 blocking peptide. *A*, *C*, and *D*, results are represented as the mean ± SD. For statistical analyses, a one-sample *t* test was used in case of normal distribution or a one-sample Wilcoxon test in the absence of normal distribution, $*p \leq 0.05$; n.s., not significant. MIF, macrophage migration inhibitory factor; N-TIMP-1, N-terminal domainof TIMP-1; TIMP-1, tissue inhibitor of metalloproteinases-1; ZAP-70, zeta chain–associated protein kinase-70.

Laboratories Inc). Dot intensity was quantified using the ImageLab Software (Bio-Rad Laboratories Inc).

Immunostaining and confocal microscopy

One hundred microgram of recombinant human TIMP-1 was fluorescently labeled using the Alexa Fluor 555 Microscale Protein Labeling Kit (cat. #A30007, Thermo Fisher Inc) according to manufacturer's instructions. For stimulation of cells with fluorescently labeled TIMP-1 or N-TIMP-1, 6×10^5 cells were stimulated with Alexa^{555}TIMP-1 (70 nM) or Alexa^{555}N-TIMP-1 (equimolar concentrated) for 10 min on ice and the nonbound ligand was rigorously washed off with ice-cold PBS (3×). Cells were fixed by 4% PFA for 15 min at RT, washed twice with PBS, and permeabilized by 0.5% Triton X-100 in PBS for 10 min at RT. After washing (2× with PBS), cells were blocked with 5% horse serum in PBS and stained for CD74 using anti-CD74 antibodies (1:500, #ab108393, Abcam) diluted in the blocking solution overnight at 4 °C. After washing (2× with PBS), cells were incubated with the secondary antibody (1:500, cat. #SA5-10038, donkey anti-rabbit IgG-DyLight488, Thermo Fisher Scientific Inc) diluted in the blocking solution for 1 h at RT. Nuclei were stained with DAPI (1:5000, #A4099, AppliChem) for 10 min at RT, mounted using ROTI-Mount FluorCare (Carl Roth) and stored at 4 °C until imaging. Imaging was performed with an inverted Leica TCS SP8 confocal microscope with White Light Laser and HyD photodetectors using a HC PL APO CS2 64×/OIL objective. Analysis of pictures and 3D surface models of nuclei and colocalization regions were performed using Imaris 9.3.1 (Oxford Instruments).

Flow cytometry

Viability of Namalwa cells treated with or without the CD74 blocking peptide C36L1 (37) (200 μM, KSSQSVFYSSNNKNYLA-NH2, peptides & elephants GmbH) was monitored by flow cytometry. Cells were starved for 24 h before stimulation in serum-free media containing 0.1% BSA. After 6 h of treatment with or without the blocking peptide, cells were transferred to 96-well v-bottom plates (TPP Techno Plastic Products AG), and dead cells were stained using 7-AAD (1:40, cat.#420403, BioLegend). Staining of cell surface CD74 was performed by incubation of cells with FITC-conjugated anti-CD74 antibodies (1:100, cat.# 11-0748-42, BioLegend) for 30 min at 4 °C and subsequent staining of dead cells using 7-AAD (1:40, cat.#420403, BioLegend). Flow cytometry was performed with the SA3800 Spectral Analyzer (Sony Biotechnology Inc) and analyzed using FlowJo Software (version.10.6., Tree Star, Inc).

In silico *molecular docking*

For *in silico* prediction of TIMP-1–CD74 complexes, the molecular docking software *Haddock* (30) (semiflexible docking) was used. The spatial coordinates for the molecular docking were retrieved from the Protein Data Bank for a 20-kDa human TIMP-1 monomer (31) (PDB ID: 1uea) and the trimerized extracellular domain of the 33-kDa isoform of human CD74 (32) (PDB ID: 1lle). For docking, the coordinates were entered as whole molecules. The coordinates for both molecules were entered in the CPORT server (47) to generate active and passive residues that are necessary for the molecular docking with Haddock. Coordinates for TIMP-1 and CD74 as whole molecules as well as the respective active and passive residues were entered in the Haddock webserver. This docking approach generated 400 complexes of TIMP-1 and CD74. 186 of these complexes clustered in 22 clusters. The three best-ranked structures (according to the energetically most favorable conformation) were utilized for further analysis and were visualized.

The three clusters with the lowest haddock score (balanced mode) were utilized for interface analysis and visualization. For interface analysis, the SpotOn webserver (33, 34) was used. The respective complex coordinates were entered as whole complexes in the SpotOn software that calculated interface residues. Comparison of the interface residues on TIMP-1 and CD74 of the different complexes was conducted by Microsoft Excel. For representation of complexes, UCSF Chimera (version 1.15) was used.

Statistical analyses

Statistical analysis was performed using the statistical software SPSS, version 24.0. Normal distribution was tested by Shapiro–Wilk tests. Groups were compared using Student's *t* test for independent samples in the case of normal distribution or the nonparametric Mann–Whitney test for independent variables in the absence of normal distribution. For Western blot densitometric analyses, a one-sample *t* test compared with the reference value 1 was used in case of normal distribution or a one-sample Wilcoxon test compared with the reference value 1 in the absence of normal distribution.

Data availability

The data supporting the findings of this study are contained within the article.

Supporting information—This article contains supporting information (35, 36).

Acknowledgments—The B cell lymphoma cell line was kindly provided by Ghislain Opdenakker (KU Leuven, Leuven, Belgium). Molecular graphics were generated with UCSF Chimera, developed by the Resource for Biocomputing, Visualization, and Informatics at the University of California, San Francisco, USA, with support from NIH P41-GM103311.

Author contributions—B. S., C. E., C. D. H., D. H., and A. K. conceptualization; B. S., C. E., and D. H. data curation; B. S., C. E., L. F., and D. H. formal analysis; B. S. and C. E. validation; B. S., C. E., L. F., S. K., R. M., F. B., C. D. H., and D. H. investigation; B. S., C. E., and D. H. visualization; B. S., C. E., L. F., S. K., R. M., F. B., J. B., C. D. H., D. H., and A. K. methodology; B. S., C. E., C. D. H., and A. K. writing–original draft; B. S., C. E., L. F., S. K., R. M., P. K., J. B., C. D. H., D. H., and A. K. writing–review and editing; P. K. and A. K.

resources; D. H. software; A. K. supervision; A. K. funding acquisition; A. K. project administration.

Funding and additional information—This work was supported by grants to A. K. from the Deutsche Forschungsgemeinschaft, Bonn, Germany (KR2047/1-3, and KR2047/8-1) and the Wilhelm Sander-Stiftung, Munich, Germany (2016.124.1 and 2016.124.2). The content is solely the responsibility of the authors and does not necessarily represent the official views of the National Institutes of Health.

Conflict of interest—The authors declare that they have no conflicts of interest with the contents of this article.

Abbreviations—The abbreviations used are: MIF, macrophage migration inhibitory factor; N-TIMP-1, N-terminal domain of TIMP-1; TIMP-1, tissue inhibitor of metalloproteinases-1; ZAP-70, zeta chain–associated protein kinase-70.

References

1. Lorente, L., Martín, M. M., Solé-Violán, J., Blanquer, J., Labarta, L., Díaz, C., Borreguero-León, J. M., Orbe, J., Rodríguez, J. A., Jiménez, A., and Páramo, J. A. (2014) Association of sepsis-related mortality with early increase of TIMP-1/MMP-9 ratio. *PLoS One* **9**, e94318
2. Nukarinen, E., Lindström, O., Kuuliala, K., Kylänpää, L., Pettilä, V., Puolakkainen, P., Kuuliala, A., Hämäläinen, M., Moilanen, E., Repo, H., and Hästbacka, J. (2016) Association of matrix metalloproteinases -7, -8 and -9 and TIMP -1 with disease severity in acute pancreatitis. A cohort study. *PLoS One* **11**, e0161480
3. Eckfeld, C., Häußler, D., Schoeps, B., Hermann, C. D., and Krüger, A. (2019) Functional disparities within the TIMP family in cancer: Hints from molecular divergence. *Cancer Metastasis Rev.* **38**, 469–481
4. Woolley, D. E., Roberts, D. R., and Evanson, J. M. (1975) Inhibition of human collagenase activity by a small molecular weight serum protein. *Biochem. Biophys. Res. Commun.* **66**, 747–754
5. Docherty, A. J., Lyons, A., Smith, B. J., Wright, E. M., Stephens, P. E., Harris, T. J., Murphy, G., and Reynolds, J. J. (1985) Sequence of human tissue inhibitor of metalloproteinases and its identity to erythroid-potentiating activity. *Nature* **318**, 66–69
6. Guedez, L., Stetler-Stevenson, W. G., Wolff, L., Wang, J., Fukushima, P., Mansoor, A., and Stetler-Stevenson, M. (1998) *In vitro* suppression of programmed cell death of B cells by tissue inhibitor of metalloproteinases-1. *J. Clin. Invest.* **102**, 2002–2010
7. Guedez, L., Martinez, A., Zhao, S., Vivero, A., Pittaluga, S., Stetler-Stevenson, M., Raffeld, M., and Stetler-Stevenson, W. G. (2005) Tissue inhibitor of metalloproteinase 1 (TIMP-1) promotes plasmablastic differentiation of a Burkitt lymphoma cell line: Implications in the pathogenesis of plasmacytic/plasmablastic tumors. *Blood* **105**, 1660–1668
8. Guedez, L., Mansoor, A., Birkedal-Hansen, B., Lim, M. S., Fukushima, P., Venzon, D., Stetler-Stevenson, W. G., and Stetler-Stevenson, M. (2001) Tissue inhibitor of metalloproteinases 1 regulation of interleukin-10 in B-cell differentiation and lymphomagenesis. *Blood* **97**, 1796–1802
9. Chesler, L., Golde, D. W., Bersch, N., and Johnson, M. D. (1995) Metalloproteinase inhibition and erythroid potentiation are independent activities of tissue inhibitor of metalloproteinases-1. *Blood* **86**, 4506–4515
10. Murphy, G., Houbrechts, A., Cockett, M. I., Williamson, R. A., O'Shea, M., and Docherty, A. J. P. (1991) The N-terminal domain of tissue inhibitor of metalloproteinases retains metalloproteinase inhibitory activity. *Biochemistry* **30**, 8097–8102
11. Jung, K.-K., Liu, X.-W., Chirco, R., Fridman, R., and Kim, H.-R. C. (2006) Identification of CD63 as a tissue inhibitor of metalloproteinase-1 interacting cell surface protein. *EMBO J.* **25**, 3934–3942
12. Warner, R. B., Najy, A. J., Jung, Y. S., Fridman, R., Kim, S., and Kim, H.-R. C. (2020) Establishment of structure-function relationship of tissue inhibitor of metalloproteinase-1 for its interaction with CD63: Implication for cancer therapy. *Sci. Rep.* **10**, 2099
13. Cui, H., Seubert, B., Stahl, E., Dietz, H., Reuning, U., Moreno-Leon, L., Ilie, M., Hofman, P., Nagase, H., Mari, B., and Krüger, A. (2015) Tissue inhibitor of metalloproteinases-1 induces a pro-tumourigenic increase of miR-210 in lung adenocarcinoma cells and their exosomes. *Oncogene* **34**, 3640–3650
14. Grünwald, B., Harant, V., Schaten, S., Frühschütz, M., Spallek, R., Höchst, B., Stutzer, K., Berchtold, S., Erkan, M., Prokopchuk, O., Martignoni, M., Esposito, I., Heikenwalder, M., Gupta, A., Siveke, J., *et al.* (2016) Pancreatic pre-malignant lesions secrete TIMP1, which activates hepatic stellate cells via CD63 signaling to create a pre-metastatic niche in the liver. *Gastroenterology* **151**, 1011–1024
15. Kobuch, J., Cui, H., Grünwald, B., Saftig, P., Knolle, P. A., and Krüger, A. (2015) TIMP-1 signaling via CD63 triggers granulopoiesis and neutrophilia in mice. *Haematologica* **100**, 1005–1013
16. Schoeps, B., Eckfeld, C., Prokopchuk, O., Böttcher, J., Häußler, D., Steiger, K., Demir, I. E., Knolle, P., Soehnlein, O., Jenne, D. E., Hermann, C. D., and Krüger, A. (2021) TIMP1 triggers neutrophil extracellular trap formation in pancreatic cancer. *Cancer Res.* **81**, 3568–3579
17. Grünwald, B., Schoeps, B., and Krüger, A. (2019) Recognizing the molecular multifunctionality and interactome of TIMP-1. *Trends Cell Biol.* **29**, 6–19
18. Moreira, J. M., Høeberg, M., Ulrik Lademann, U., Viuff, B., Jensen, L. V., Stenvang, J., Nygård, S. B., Ørum-Madsen, M. S., Vistesen, M. V., Fuglsang, A. T., Liu, S., and Brünner, N. (2015) Identification and characterization of a new TIMP-1 binding protein [abstract]. *Cancer Res.* **75**. Abstract nr P5-07-08
19. Farr, L., Ghosh, S., and Moonah, S. (2020) Role of MIF cytokine/CD74 receptor pathway in protecting against injury and promoting repair. *Front. Immunol.* **11**, 1273
20. Stein, R., Mattes, M. J., Cardillo, T. M., Hansen, H. J., Chang, C.-H., Burton, J., Govindan, S., and Goldenberg, D. M. (2007) CD74: A new candidate target for the immunotherapy of B-cell neoplasms. *Clin. Cancer Res.* **13**, 5556s–5563s
21. Borghese, F., and Clanchy, F. I. L. (2011) CD74: An emerging opportunity as a therapeutic target in cancer and autoimmune disease. *Expert Opin. Ther. Targets* **15**, 237–251
22. Vandenbark, A. A., Meza-Romero, R., and Offner, H. (2020) Surviving the storm: Dealing with COVID-19. *Cell. Immunol.* **354**, 104153
23. Schröder, B. (2016) The multifaceted roles of the invariant chain CD74–more than just a chaperone. *Biochim. Biophys. Acta* **1863**, 1269–1281
24. Stockinger, B., Pessara, U., Lin, R. H., Habicht, J., Grez, M., and Koch, N. (1989) A role of Ia-associated invariant chains in antigen processing and pressentation. *Cell* **56**, 683–689
25. Shachar, I., and Flavell, R. A. (1996) Requirement for invariant chain in B cell maturation and function. *Science* **274**, 106–108
26. Roche, P. A., Marks, M. S., and Cresswell, P. (1991) Formation of a nine-subunit complex by HLA class II glycoproteins and the invariant chain. *Nature* **354**, 392–394
27. Koch, N., Koch, S., and Hämmerling, G. J. (1982) Ia invariant chain detected on lymphocyte surfaces by monoclonal antibody. *Nature* **299**, 644–645
28. Leng, L., Metz, C. N., Fang, Y., Xu, J., Donnelly, S., Baugh, J., Delohery, T., Chen, Y., Mitchell, R. A., and Bucala, R. (2003) MIF signal transduction initiated by binding to CD74. *J. Exp. Med.* **197**, 1467–1476
29. Klasen, C., Ohl, K., Sternkopf, M., Shachar, I., Schmitz, C., Heussen, N., Hobeika, E., Levit-Zerdoun, E., Tenbrock, K., Reth, M., Bernhagen, J., and El Bounkari, O. (2014) MIF promotes B cell chemotaxis through the receptors CXCR4 and CD74 and ZAP-70 signaling. *J. Immunol.* **192**, 5273–5284
30. van Zundert, G. C. P., Rodrigues, J. P. G. L. M., Trellet, M., Schmitz, C., Kastritis, P. L., Karaca, E., Melquiond, A. S. J., van Dijk, M., de Vries, S. J., and Bonvin, A. M. J. J. (2016) The HADDOCK2.2 web server: User-friendly integrative modeling of biomolecular complexes. *J. Mol. Biol.* **428**, 720–725
31. Gomis-Rüth, F. X., Maskos, K., Betz, M., Bergner, A., Huber, R., Suzuki, K., Yoshida, N., Nagase, H., Brew, K., Bourenkov, G. P., Bartunik, H., and

Bode, W. (1997) Mechanism of inhibition of the human matrix metalloproteinase stromelysin-1 by TIMP-1. *Nature* **389**, 77–81
32. Jasanoff, A., Wagner, G., and Wiley, D. C. (1998) Structure of a trimeric domain of the MHC class II-associated chaperonin and targeting protein Ii. *EMBO J.* **17**, 6812–6818
33. Melo, R., Fieldhouse, R., Melo, A., Correia, J. D. G., Cordeiro, M. N. D. S., Gümüş, Z. H., Costa, J., Bonvin, A. M. J. J., and Moreira, I. S. (2016) A machine learning approach for hot-spot detection at protein-protein interfaces. *Int. J. Mol. Sci.* **17**, 1215
34. Moreira, I. S., Koukos, P. I., Melo, R., Almeida, J. G., Preto, A. J., Schaarschmidt, J., Trellet, M., Gümüş, Z. H., Costa, J., and Bonvin, A. M. J. J. (2017) SpotOn: High accuracy identification of protein-protein interface hot-spots. *Sci. Rep.* **7**, 8007
35. Meza-Romero, R., Benedek, G., Leng, L., Bucala, R., and Vandenbark, A. A. (2016) Predicted structure of MIF/CD74 and RTL1000/CD74 complexes. *Metab. Brain Dis.* **31**, 249–255
36. Uhlén, M., Fagerberg, L., Hallström, B. M., Lindskog, C., Oksvold, P., Mardinoglu, A., Sivertsson, Å., Kampf, C., Sjöstedt, E., Asplund, A., Olsson, I., Edlund, K., Lundberg, E., Navani, S., Szigyarto, C. A.-K., *et al.* (2015) Proteomics. Tissue-based map of the human proteome. *Science* **347**, 1260419
37. Figueiredo, C. R., Azevedo, R. A., Mousdell, S., Resende-Lara, P. T., Ireland, L., Santos, A., Girola, N., Cunha, R. L. O. R., Schmid, M. C., Polonelli, L., Travassos, L. R., and Mielgo, A. (2018) Blockade of MIF-CD74 signalling on macrophages and dendritic cells restores the antitumour immune response against metastatic melanoma. *Front. Immunol.* **9**, 1132
38. Thevenard, J., Verzeaux, L., Devy, J., Etique, N., Jeanne, A., Schneider, C., Hachet, C., Ferracci, G., David, M., Martiny, L., Charpentier, E., Khrestchatisky, M., Rivera, S., Dedieu, S., and Emonard, H. (2014) Low-density lipoprotein receptor-related protein-1 mediates endocytic clearance of tissue inhibitor of metalloproteinases-1 and promotes its cytokine-like activities. *PLoS One* **9**, e103839
39. Verzeaux, L., Belloy, N., Thevenard-Devy, J., Devy, J., Ferracci, G., Martiny, L., Dedieu, S., Dauchez, M., Emonard, H., Etique, N., and Devarenne-Charpentier, E. (2017) Intrinsic dynamics study identifies two amino acids of TIMP-1 critical for its LRP-1-mediated endocytosis in neurons. *Sci. Rep.* **7**, 5375
40. Rapti, M., Atkinson, S. J., Lee, M. H., Trim, A., Moss, M., and Murphy, G. (2008) The isolated N-terminal domains of TIMP-1 and TIMP-3 are insufficient for ADAM10 inhibition. *Biochem. J.* **411**, 433–439
41. Murphy, G. (2011) Tissue inhibitors of metalloproteinases. *Genome Biol.* **12**, 233
42. Raeeszadeh-Sarmazdeh, M., Greene, K. A., Sankaran, B., Downey, G. P., Radisky, D. C., and Radisky, E. S. (2019) Directed evolution of the metalloproteinase inhibitor TIMP-1 reveals that its N- and C-terminal domains cooperate in matrix metalloproteinase recognition. *J. Biol. Chem.* **294**, 9476–9488
43. Huang, W., Suzuki, K., Nagase, H., Arumugan, S., van Doren, S. R., and Brew, K. (1996) Folding and characterization of the amino-terminal domain of human tissue inhibitor of metalloproteinases-1 (TIMP-1) expressed at high yield in E. coli. *FEBS Lett.* **384**, 155–161
44. Martin, P., Furman, R. R., Rutherford, S., Ruan, J., Ely, S., Greenberg, J., Coleman, M., Goldsmith, S. J., and Leonard, J. P. (2015) Phase I study of the anti-CD74 monoclonal antibody milatuzumab (hLL1) in patients with previously treated B-cell lymphomas. *Leuk. Lymphoma* **56**, 3065–3070
45. Huberts, D. H. E. W., and van der Klei, I. J. (2010) Moonlighting proteins: An intriguing mode of multitasking. *Biochim. Biophys. Acta* **1803**, 520–525
46. Seubert, B., Grünwald, B., Kobuch, J., Cui, H., Schelter, F., Schaten, S., Siveke, J. T., Lim, N. H., Nagase, H., Simonavicius, N., Heikenwalder, M., Reinheckel, T., Sleeman, J. P., Janssen, K.-P., Knolle, P. A., *et al.* (2015) Tissue inhibitor of metalloproteinases (TIMP)-1 creates a premetastatic niche in the liver through SDF-1/CXCR4-dependent neutrophil recruitment in mice. *Hepatology* **61**, 238–248
47. de Vries, S. J., and Bonvin, A. M. J. J. (2011) CPORT: A consensus interface predictor and its performance in prediction-driven docking with HADDOCK. *PLoS One* **6**, e17695